Life Sciences 233 (2019) 116702

Contents lists available at ScienceDirect

Life Sciences

journal homepage: www.elsevier.com/locate/lifescie

Chronic iron overload intensifies atherosclerosis in apolipoprotein E deficient mice: Role of oxidative stress and endothelial dysfunction

Vinícius Bermond Marques[a,b], Marcos André Soares Leal[a], Jandinay Gonzaga Alexandre Mageski[a], Helbert Gabriel Fidelis[a], Breno Valentim Nogueira[c], Elisardo Corral Vasquez[a,d], Silvana dos Santos Meyrelles[a], Maylla Ronacher Simões[a], Leonardo dos Santos[a,*]

[a] Department of Physiological Sciences, Federal University of Espirito Santo, Vitoria, Brazil
[b] Nursing Course, Faculdade Pitágoras, Guarapari, ES, Brazil
[c] Department of Morphology, Federal University of Espirito Santo, Vitoria, ES, Brazil
[d] Pharmaceutical Sciences Graduate Program, Vila Velha University, Vila Velha, ES, Brazil

ARTICLE INFO

Keywords:
Iron overload
Atherosclerosis
Endothelial dysfunction
Oxidative stress
Prostanoids

ABSTRACT

Aims: We previously demonstrated that iron overload induces endothelial dysfunction and oxidative stress, which could increase the risk for atherosclerosis. However, the iron-related harmfulness under a genetic predisposition to atherosclerosis is still unclear. Here, we have tested the hypothesis that chronic iron overload may change vascular reactivity associated with worsening of the atherosclerotic process in apolipoprotein E knockout (apoE(−/−)) mice.

Main methods: Serum and aortas of wild-type (WT) and apoE(−/−) mice injected with iron-dextran (IO, 10 mg/mouse/day, ip) or saline 5 times a week for 4 weeks, were used.

Key findings: Iron overload increased serum levels of iron and biomarkers of liver injury and oxidative stress, and iron deposition in the aorta in both lines, but only apoE(−/−) IO mice had intensified hypercholesterolemia and atherosclerosis. By scanning electron microscopy, the small endothelial structural damage caused by iron in WT was worsened in the apoE(−/−) group. However, endothelial dysfunction was found only in the apoE(−/−) IO group, identified by impaired relaxation to acetylcholine and hyperreactivity to phenylephrine associated with reduced nitric oxide modulation. Moreover, tiron and indomethacin attenuated reactivity to phenylephrine with greater magnitude in aortas of the apoE(−/−) IO group. Confirming, there were changes in the antioxidant (superoxide dismutase and catalase) activity, increased expression of cyclooxygenase-2 in the aorta and elevated levels of thromboxane A2 and prostacyclin metabolites in the urine of apoE(−/−) IO.

Significance: Our results showed that chronic iron overload intensifies the atherosclerotic process and induces endothelial dysfunction in atherosclerotic mice, probably due to the oxidative stress and the imbalance between the relaxing and contractile factors synthesized by the damaged endothelium.

1. Introduction

Iron is an essential metal for cellular homeostasis, participating in many physiological processes due to its ability to donate and receive electrons [1–3]. However, in situations of both primary (hereditary) and secondary (acquired) origins, there may be iron overload with consequent increase of circulating levels and deposits in different tissues [4]. These conditions are often associated with endocrine, hepatic and cardiovascular dysfunctions [5–7].

It is well established that iron overload induces cardiovascular damage through oxidative stress [5,6,8,9]. Moreover, the increased generation of reactive oxygen species (ROS) in the vasculature is associated with endothelial dysfunction in both human and experimental models of iron overload [5,10,11]. In this regard, we have previously demonstrated that iron overload in rats causes endothelial dysfunction as a function of increased ROS and decreased nitric oxide (NO) bioavailability in both conductance and resistance arteries [8,9,12].

Oxidative stress and endothelial dysfunction are closely associated with various cardiovascular diseases, not only due to changes in vascular tonus but also by increasing leukocyte adhesion and lipid

* Corresponding author at: Departamento de Ciências Fisiológicas, Centro de Ciências da Saúde, UFES, Av. Marechal Campos 1468, 29040-095 Vitória, ES, Brazil.
E-mail address: leonardo.santos@ufes.br (L. dos Santos).

https://doi.org/10.1016/j.lfs.2019.116702
Received 16 April 2019; Received in revised form 24 July 2019; Accepted 25 July 2019
Available online 26 July 2019
0024-3205/

peroxidation, thus contributing to atherosclerosis [13]. Interestingly, although iron is capable of inducing these mentioned changes, the role of iron overload per se in the atherogenesis (termed the "iron hypothesis") has been questioned due to conflicting results obtained in both animal and human studies [14–19].

Because a dynamic interaction exists between endothelial function and atherosclerosis, and both of which may be influenced by oxidative stress, we propose that endothelial dysfunction could be a potential mechanism by which iron overload intensifies atherosclerosis instead of generates it, thereby increasing the risk of cardiovascular events. In the present study we tested whether chronic iron overload can induce not only structural but also functional damage to the vascular endothelium of apoE$^{-/-}$ mice, in association with exacerbation of the atherosclerotic process.

2. Material and methods

2.1. Animals and treatments

The experiments were conducted in adult (5-months-old, 22-25 g) females apolipoprotein E knockout (apoE$^{-/-}$) mice that had a C57BL/6J genetic background, and in wild-type (WT) mice, which were kept in cages with free access to water and standard rodent feed under conditions of controlled temperature and humidity and were subject to a 12 h light-dark cycle. It was previously demonstrated that female apoE$^{-/-}$ mice spontaneously develop hypercholesterolemia and atherosclerosis at this age even without high fat diet [20]. All experiments were conducted in accordance with the Brazilian Guidelines for the Care and Use of Animals for Scientific and Educational Purposes and were approved by the Institutional Ethics Committee on Animal Use (86/2015 CEUA-UFES).

Animals were distributed into four groups: WT control (WT Ct, $n = 16$); WT with chronic iron overload (WT IO, $n = 16$); apoE$^{-/-}$ control (apoE$^{-/-}$ Ct, $n = 26$); and apoE$^{-/-}$ with chronic iron (apoE$^{-/-}$ IO, $n = 27$). The iron overload model was done as previously described [21,22]: daily intraperitoneal injections of iron-dextran (Ferrodex®, Fabiani Ltda, São Paulo, Brazil) at 10 mg/mouse, 5 days a week for 4 weeks, while the control group received saline isotonic solution for the same period and the same enforcement regime as the IO group. Animals from each lineage were randomly distributed for Ct or IO groups, and all evaluations were done by one observer blinded to the animal group.

2.2. Euthanasia and sample preparation

At the end of the treatment, the mice were anaesthetized with xylazine (10 mg/Kg, ip) plus ketamine (80 mg/Kg, ip). Blood samples were collected with guillotine exsanguination and serum aliquots were separated by centrifugation at 1400 G. Samples were stored at −80 °C until the day of analysis. The aortas were dissected, and the connective tissue was removed. For vascular reactivity study, only the thoracic aorta was used. For morphological analysis the arch and thoracic aorta were fixed in Karnovsky. Meanwhile, other aortas were frozen at −80 °C for analysis of protein expression, NO production and antioxidant enzymes activity assays.

2.3. Serum measures

The serum iron was measured in duplicate by a modified Goodwin colorimetric method with the use of commercial colorimetric kit (Bioclin, Belo Horizonte, Brazil). Cholesterol was determined by enzymatic colorimetric method (CHOD - PAP), while the activities of the liver injury biomarkers glutamic-oxaloacetic transaminase (GOT) and glutamic-pyruvic transaminase (GPT) were evaluated by Reitmamm and Frankel method and commercial colorimetric kits were used for all analyses (Bioclin, Belo Horizonte, Brazil). Malondialdehyde (MDA) was measured using a colorimetric method previously described [23] to estimate thiobarbituric acid reactive substances (TBAR), products of lipid peroxidation; and advanced oxidation protein products (AOPP) assay was used to evaluate the oxidation of proteins [24].

2.4. Analysis of atherosclerotic plaque and iron deposit in aortic arch

After 24 h of fixation with Karnovsky, the arcs aortic were immersed in Krebs-HEPES buffer (in mM: 130 NaCl, 5.6 KCl, 2 $CaCl_2$, 0.24 $MgCl_2$, 8.3 HEPES, and 11 glucose, pH 7.4) with 30% sucrose for 1 h, then embedded in inclusion medium for cryostat (Killik ®, Easy Path). The sections of the aortic arch were cut in a cryostat at 10 μm thickness and transferred to gelatinized slides, and were frozen until the time of protocol.

On the day of protocol, the slides were kept in an oven at 37 °C for 1 h to remove the inclusion medium and fixed on the slide with ice-cold acetone. Tissue iron deposits were visualized in sections of the aortic arch stained with Prussian blue (Mallory's method), and atherosclerotic plaque was marked with *Oil-Red-O* staining. For cell counting into the plaques, toluidine blue was used to stain nuclei. Histological sections were examined with optical microscope coupled to a camera for image acquisition.

2.5. Scanning electron microscopy

Scanning electron microscopy was performed by methods previously described [25]. After fixation of the aorta with Karnovsky-cacodylate buffer for 24 h, and post-fixed in a solution of 1% osmium tetroxide, 1.25% potassium ferrocyanide and 0.2 M cacodylate buffer (solution B) for 1 h, the samples were then washed in cacodylate buffer (0.1 M) and ultrapure water and cut open, in longitudinal sections under a stereomicroscope, dehydrated in ascending grades of ethanol, and critical-point dried with liquid CO_2. The specimens were mounted on stubs sputter coated with 10 nm of pure gold and examined using a scanning electron microscope (Jeol, JEM6610 LV, Jeol Inc., USA). For each specimen, four photomicrographs were randomly taken at ×2000 magnification.

2.6. Vascular reactivity protocols

Aortic segments (2 mm in length) were mounted in a small-vessel dual chamber myograph for measurement of isometric tension [26], containing an organ bath with Krebs-Henseleit solution (KHS, in mM: 115 NaCl, 25 $NaHCO_3$, 4.7 KCl, 1.2 $MgSO_4$ $7H_2O$, 2.5 $CaCl_2$, 1.2 KH_2PO_4, 11.1 glucose, and 0.01 Na_2 EDTA) at a temperature of 37 °C gassed with 95% de O_2 and 5% CO_2 (pH 7.4). Segments were stretched to their optimal lumen diameter for active tension development. After a 45-min equilibration period, aortas were exposed to 120 mM KCl to check their functional integrity. To verify the functional integrity of the endothelium a relaxation curve induced by acetylcholine (ACh, 10^{-10} to 3.10^{-4} M) was performed in aortic rings precontracted with phenylephrine at concentration that produce approximately 50–70% of the contraction induced by 120 mM KCl in each case. After 60 min washout, concentration-response curves to phenylephrine (10^{-10} to 3.10^{-4} M) were determined, and after new stabilization period, curves concentration responses to sodium nitroprusside (10^{-10} to 3.10^{-4} M) were constructed to evaluate the endothelium-independent relaxation. Additionally, the role of endothelium-derived vasoactive factors was investigated by pre-incubating a nonspecific NO synthase inhibitor N-nitro-L-arginine methyl ester (L-NAME, 100 μM), a superoxide anion scavenger (tiron, 1 mM) or a nonspecific cyclooxygenase (COX) inhibitor (indomethacin, 10 μM) 30 min before phenylephrine.

2.7. Vascular nitric oxide production

NO production was determined using 4,5-diaminofluorescein

diacetate (DAF-2) as previously described [9]. Aortas were dissected and embedded in freezing medium. Transverse arterial sections (10 μm) were obtained by cryostat, collected on glass slides incubated at 37 °C under the same conditions of the vascular reactivity protocol for 30 min with 0.1 M phosphate buffer containing $CaCl_2$ (0.45 mM) and phenylephrine (10^{-4} M), in the absence and presence of L-NAME (100 μM) to evaluate specific NO-dependent fluorescence. The slides were dried and incubated for 30 min at 37 °C in a light-protected humidified chamber with 8 μM DAF-2 diluted in phosphate buffer solution containing $CaCl_2$ and phenylephrine (10^{-4} M). After 30 min, digital images were collected on the Leica DM 2500 fluorescence microscope and Leica DFC 310 X camera, using the same image configuration for Ct and IO groups. For quantification, 5 segments of the aorta per animal were used to obtain the sample mean. The mean fluorescence density was calculated using Image J. software 1.44p.

2.8. Activity of antioxidant enzymes in aorta

Proteins from homogenized aortas were used to measure the activity of antioxidant enzymes. The enzymatic activity of catalase was evaluated by the decay of the absorbance after addition of hydrogen peroxide, which occurs through the enzyme catalase. During the protocol, 50 μL of sample and 5 μL of 10% triton were pipetted into an eppendorf, vortexed and held for 15 min on ice to release the catalase. 240 μL of 10 mM phosphate buffer pH 7.0 was then added to each well and the spectrum was cleared. Then, in duplicate, 10 μL of sample and 240 μL of medium were pipetted with hydrogen peroxide (room temperature) and waited 2 min for reading at 240 nm for 30 min, with a reading every 30 s.

Already SOD activity, was evaluated with a method that is based on the inhibition of the auto-oxidation of adrenaline by SOD. Adrenaline when added in basic media reacts with the superoxide anion and forms the adrenochrome which exhibits maximum absorption at 480 nm. Thus, the lower the absorbance of the adrenochrome, the greater the ability of SOD to dismantle the superoxide anion and inhibit the auto-oxidation reaction, thus reflecting its activity by an indirect method. To this end, 190 μL of glycine buffer and 10 μL of sample was added and the spectrum was cleared. After, 5 μL of adrenaline was pipetted into each well, immediately read at 480 nm for 10 min, every 40 s.

2.9. Western blot analysis

Proteins from homogenized aortas (80 μg) were separated by 10% SDS-PAGE and subsequently transferred to nitrocellulose membranes that were exposed to the primary monoclonal antibody anti-COX-2 (1:1000, Cayman Chemical, Ann Arbor, MI, USA). After being washed, membranes were incubated with anti-mouse immunoglobulin antibody conjugated to horseradish peroxidase (1:5000; Sigma Aldrich, St. Louis, MO, USA). After being washed thoroughly, immunocomplexes were detected using an enhanced hoseradish peroxidase/luminol chemiluminescence system (ECL Plus; GE Healthcare, Buckinghamshire, UK) and immunodetection was carried out using ChemiDoc system (Bio-Rad Laboratories, Inc., Hercules, CA, USA). Signals on the immunoblot were quantified using the ImageJ computer program. The same membrane was used to determine α-actin (1:20000, Sigma Aldrich, St. Louis, MO, USA) expression. Protein expression data are expressed as the ratio between signals on the immunoblot corresponding to the studied protein and α-actin.

2.10. Measurement of thromboxane and prostacyclin metabolites in the urine

The level of 11-deydro thromboxane B_2 (TXB_2) and prostaglandin I metabolites (PGIM) in urine collected for 24 h were quantified using a competitive enzyme immunoassay kit to estimate systemic production of TXA_2 and PGI_2, respectively. All urinary prostanoid metabolites measures were normalized for the creatinine content in the same sample. The TXB_2 (No 519510) and PGIM (No 501100) kits were purchased from Cayman Chemical (Ann Arbor, MI, USA), and creatinine obtained from Bioclin (Belo Horizonte, MG, Brazil).

2.11. Drugs and chemicals

Salts and reagents used, when not otherwise indicated, were purchased from Sigma and Merck (Darmstadt, Germany).

2.12. Statistical analyses

Vasoconstrictor responses induced by phenylephrine were expressed as force normalized by the ring size (mN/mm). Vasodilator responses are expressed as a percentage of the previous contraction. For each concentration-response curve, the maximum effect (R_{max}) and the concentration of agonist that produced one-half of R_{max} (EC_{50}) were calculated using nonlinear regression analysis with a sigmoid construction. The sensitivity of the agonists was expressed as pD_2 ($-\log EC_{50}$). To compare the effects of drug incubation on the contractile responses to phenylephrine, the results were expressed as difference between the areas under the concentration-response curves (dAUC) with and without incubation. For COX-2 protein expression, data are expressed as the ratio of the α-actin expression. Results are expressed as means ± SEM of the number of mice indicated; differences were analyzed using Student's *t*-test or two-way ANOVA followed by Fisher's Least Significant Difference (LSD) test for multiple comparisons. For all inferences, significance was considered when $p < 0.05$. Statistical analysis and graph construction were performed using GraphPad Prism version 6.0 for Windows (GraphPad Software, La Jolla, CA, USA).

3. Results

3.1. Chronic iron overload intensifies hypercholesterolemia in atherosclerotic mice

At the end of the treatment, all animals injected with iron had a characteristic phenotype of experimental models with chronic overload, such as hyperpigmentation of the skin and internal organs, increased liver weight and elevation of serum iron and biomarkers of liver injury (GOT and GPT), without significant difference between the lineages (Table 1).

As showed in Table 1, $apoE^{-/-}$ Ct mice had elevated total cholesterol compared to WT Ct. However, chronic iron overload potentiated the hypercholesterolemia of $apoE^{-/-}$ IO compared to $apoE^{-/-}$ Ct (Table 1). Moreover, these impairment on the lipemic profile of the $apoE^{-/-}$ was associated with changes on the systemic oxidative stress: both serum MDA and AOPP levels, indicative of lipid peroxidation and protein oxidation respectively, were increased by iron treatment in both lineages, but in a greater extent in the $apoE^{-/-}$ IO group (Table 1).

3.2. Iron overload intensifies atherosclerotic process in $apoE^{-/-}$ mice

As expected, group WT Ct mice did not present atherosclerotic plaques. Similarly, there was no atherosclerosis in aortas from the WT IO group. However, the $apoE^{-/-}$ Ct group showed small to moderate atherosclerotic plaques, but iron overload significantly enhanced plaque formation in $apoE^{-/-}$ mice (Fig. 1A and B) with increased cell infiltrate (supplementary figure S1). In addition, iron overload induced iron deposit in the aorta wall and in the $apoE^{-/-}$ IO group atheroma plate had significant iron deposition (Fig. 1C and D).

3.3. Iron overload alters endothelial layer architecture in atherosclerotic mice

We used scanning electronic microscopy to assess possible structural

Table 1
Serum parameters and body weight of iron-injected mice.

	WT		apoE$^{-/-}$	
	Control	Iron	Control	Iron
Serum iron (μg/dL)	80 ± 13 (6)	6301 ± 523 (8) *	70.01 ± 8 (4)	5673 ± 588 (8) *
Cholesterol (mg/dL)	63 ± 5 (11)	84 ± 4 (14)	383 ± 28 (14) #	651 ± 37 (15) *#
MDA (μM)	1.51 ± 0.2 (6)	2.19 ± 0.2 (7) *	1.56 ± 0.1 (10)	2.9 ± 0.24 (10)*#
AOPP (μM cloramine-T)	11.1 ± 0.4 (4)	133.3 ± 20 (3) *	61.8 ± 11 (8)	295.7 ± 50 (6) *#
GOT (UI)	25 ± 3 (8)	51 ± 5 (8) *	24 ± 3 (6)	52 ± 13 (4) *
GPT (UI)	6.2 ± 0.3 (8)	56 ± 10 (8) *	5.6 ± 0.2 (7)	37 ± 5 (4) *
Body weight (g)	24.5 ± 0.5 (14)	25.9 ± 0.3 (16)	24.7 ± 0.5 (9)	25.2 ± 0.3 (18)

MDA: malondialdehydes; AOPP: advanced oxidation protein products; GOT: glutamic-oxaloacetic transaminase; GPT: glutamic-pyruvic transaminase; WT: wild-type. Values are expressed as means ± SEM. $^{*}P < 0.05$ IO vs. Ct within the same lineage and $^{\#}P < 0.05$ apoE$^{-/-}$ vs. WT within the same experimental condition, by using two-way ANOVA and Fisher's test for multiple comparisons. The number of animals used is indicated in parentheses.

changes on the endothelial cell surface. As shown in Fig. 2, electronmicrographs of the thoracic aortas from WT Ct mice showed a regular and confluent endothelium. However, in the WT IO group it was possible to identify the beginning of the structural lesion in the superficial luminal layer (endothelial surface disruption with appearance of superficial vacuoles or blebs). Moreover, besides the changes observed in the WT IO, there were also remarkable damage in regularity and endothelial confluence in the apoE$^{-/-}$ Ct group. In the apoE$^{-/-}$ IO group, in addition to the aforementioned alterations, the presence of several leukocytes adhered to the endothelial surface characterized a more severe morphological damage induced by iron in this lineage.

3.4. Iron overload induces endothelial dysfunction via reactive oxygen species and cyclooxygenase pathway

Due to the structural damage identified on the endothelium surface, we used *in vitro* vascular reactivity protocols to evaluate de degree of functional change induced by iron overload in both lineages. The endothelium-independent relaxing response to nitric oxide donor sodium nitroprusside was similar between groups (Fig. 3B). Moreover, although the WT IO and apoE$^{-/-}$ groups have morphological changes on the endothelial cell surface, the endothelium-dependent relaxation to acetylcholine was significant impaired only in the apoE$^{-/-}$ IO group (Fig. 3C and supplementary table S1) and contractile response to phenylephrine was increased only in the apoE$^{-/-}$ IO group (Fig. 3A).

To evaluate the influence of endothelial factors on the response to

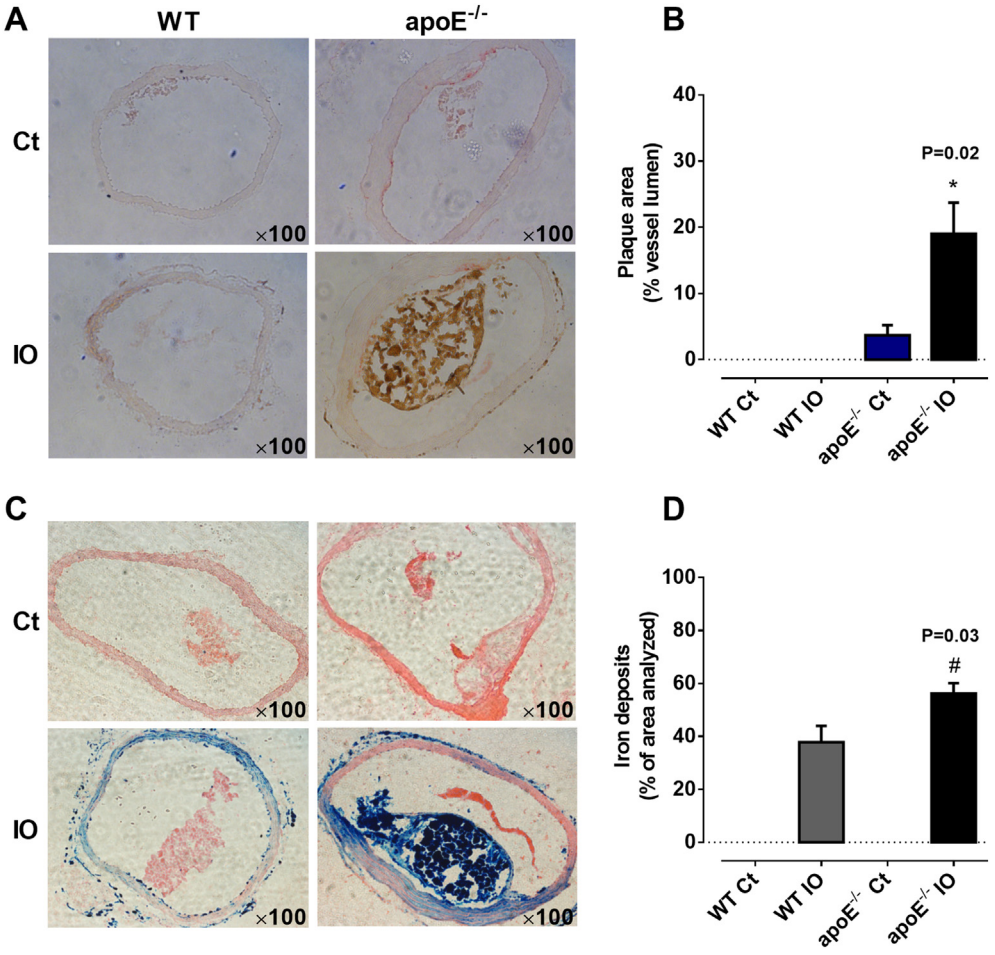

Fig. 1. Increased atherosclerotic plaque and iron deposits in the aortic arch of apoE$^{-/-}$ mice after iron overload. In A, sections of the aortic arch representing lipid deposition (in red) demonstrated by *Oil-Red-O* staining. In B, bar graph demonstrating quantitative analysis of plaque extension, as percent of vessel lumen. Iron deposits (in blue) are visualized by Prussian blue staining (C). In D, bar graph demonstrating quantitative analysis of iron deposits, as percent of area. Aortic arch sections representative of the control (Ct) and iron (IO) groups, in the wild-type (WT) and apoE$^{-/-}$ lineages. Original magnification × 100. Data are expressed as mean ± SEM. $^{*}P < 0.05$ IO vs. Ct within the same lineage and $^{\#}P < 0.05$ apoE$^{-/-}$ vs. WT within the same experimental condition, by using Student's *t*-test. Sample number of 4–6 per group. (For interpretation of the references to colour in this figure legend, the reader is referred to the web version of this article.)

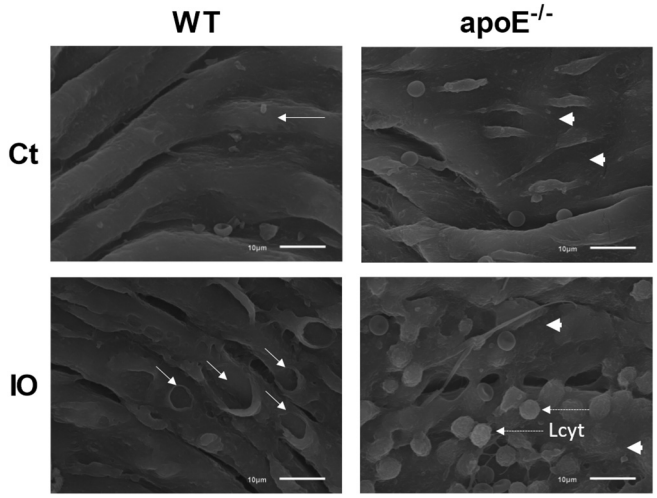

Fig. 2. Effects of chronic iron overload on the endothelial surface architecture. Scanning electron microscopy showing representative endothelial structure of aortas from the control (Ct) and iron overload (IO) in the wild-type (WT) and apoE$^{-/-}$ lineages. *Scale bar* 10 μm. Long arrow: endothelial cell; short arrow: vacuoles or blebs; arrow head: damage in regularity and endothelial confluence; dotted arrow: leukocyte (Lcyt).

phenylephrine, protocols incubating inhibitors were done. The NO synthase inhibition with L-NAME increased contractions to phenylephrine of the aortas from all groups (Fig. 3D and E and supplementary table S2), but in a lesser extent in the apoE$^{-/-}$ IO group, as demonstrated by the dAUC (Fig. 3F).

Incubation with indomethacin (10 μM) reduced vascular reactivity in all groups (Fig. 3G and H), but in a greater magnitude in the apoE$^{-/-}$ IO group (Fig. 3I). Moreover, the reactive oxygen species scavenger tiron reduce the vasocontractile response to phenylephrine only in the apoE$^{-/-}$ IO group (Fig. 3J and L) restoring the vascular reactivity to values similar to the apoE$^{-/-}$ Ct group. Taken together, our data suggest an important role of COX and oxidative stress in the endothelial dysfunction and altered vascular reactivity in atherosclerotic mice submitted to iron overload.

3.5. Iron overload decreases local NO production in atherosclerotic mice

Because the reduced modulation of NO in the vascular reactivity to phenylephrine was observed solely in the apoE$^{-/-}$ IO group, the evaluation of in situ production and/or bioavailability of NO were restricted to aortic rings from the groups with apoE$^{-/-}$ lineage. Corroborating the functional data, the NO sensitive fluorescence was reduced in the apoE$^{-/-}$ IO, and L-NAME was able to reduce the fluorescence in the apoE$^{-/-}$ Ct but not in the apoE$^{-/-}$ IO, indicating reduced NO production and/or bioavailability (Fig. 4).

3.6. Iron overload increases cyclooxygenase-derived prostanoids and induces oxidative stress in the aorta of atherosclerotic mice

As shown in Fig. 5C and D, the amount of prostanoid metabolites PGIM and TXB_2 increased significantly in the urine of apoE$^{-/-}$ IO mice. Corroborating, an increase of the COX-2 protein expression was found in aortas from apoE$^{-/-}$ IO compared to the apoE$^{-/-}$ Ct group (Fig. 5E).

Because iron overload was able to increase serum MDA and AOPP levels in greater magnitude in the apoE$^{-/-}$ lineage, and since tiron attenuated vasoconstriction to phenylephrine only in the apoE$^{-/-}$ IO group, we assessed the activity of antioxidant enzymes in the aorta. Catalase and superoxide dismutase activity decreased in the aorta of apoE$^{-/-}$ IO group compared to the apoE$^{-/-}$ Ct (Fig. 5A and B).

4. Discussion

In the present study, we investigated the effects of chronic iron overload on endothelial function and structure, in association with atherogenesis in the apoE$^{-/-}$ mouse. All animals injected with iron-dextran, regardless the lineage, had increased serum iron levels and hyperpigmentation of the skin and internal organs as phenotypic characteristics of iron overload, similar to other studies that used the same treatment scheme [11,21,22,27].

Depending on gender and age, apoE$^{-/-}$ mice may develop hypercholesterolemia and spontaneous atherosclerosis [20]. Confirming this phenotype, the apoE$^{-/-}$ group had an increase in total cholesterol (6.1-fold). Interestingly, iron was able to potentiate hypercholesterolemia in apoE$^{-/-}$ mice, without significantly changes in WT animals. Iron overload is often associated with hepatic injury [28,29], and in fact, serum markers of liver damage GOT and GPT were elevated in both lineages we injected with iron-dextran. Thus, we could speculate that the combination of the altered cholesterolemic state due to apoE$^{-/-}$ deficiency and the liver damage due to iron overload intensified the hypercholesterolemia in knockout mice. In addition, because serum markers of oxidative stress MDA and AOPP were also elevated by iron treatment in greater magnitude in the apoE$^{-/-}$ mice, it is also suggested a possible contribution of the oxidative stress for the exacerbated hypercholesterolemia. Actually, increased oxidative stress due to iron overload have been described in several clinical and experimental studies as the key mediator of organ damage [5,9,10].

As expected, the WT mice did not show atheroma plaque in their aortas, but the apoE$^{-/-}$ Ct group had atheroma plaque (occupying approximately 4% of the aorta lumen) corroborating previous evidences of atherosclerosis in adult apoE$^{-/-}$ mice even when fed normal chow (non hypercholesterolemic) [30,31]. Notwithstanding, iron overload intensified atherosclerotic plaque formation in apoE$^{-/-}$ IO mice (approximately 19% of the aorta lumen) and increased cell infiltrate into the plaques compared to the apoE$^{-/-}$ Ct. Interestingly, other studies in apoE$^{-/-}$ mice show that high-iron diet was not atherogenic [16] and even decreased the atherosclerosis progression [17]. Despite these conflicting data about the relationship between iron and atherogenesis, the higher dose of iron burden and the different route of overload could explain the particular scenario of the present study. Actually, our findings reinforce previous evidences of augmented atherosclerosis in apoE$^{-/-}$ mice [14] and hypercolesterolemic rabbits [15] chronically injected with parenteral iron-dextran. Furthermore, iron chelation with desferrioxamine attenuated the atherogenesis in rabbits [32] and both iron chelation or iron-deficient diet reduced atherosclerosis plaque formation in apoE$^{-/-}$ mice [33,34] even in the absence of iron overload. Recently, Vinchi et al. (2019) demonstrated that, in a genetic model of Type IV hereditary hemochromatosis in the apoE$^{-/-}$ mouse background, iron overload aggravated, while iron chelation attenuated the atherosclerosis [35], which strength the role of circulating iron on the atherosclerosis progression.

We detected Prussian blue-positive deposits on the aortic wall including endothelial spots and significant iron deposition in the adventitia of the WT IO and apoE$^{-/-}$ IO groups. Moreover, although iron has been identified in human atherosclerotic lesions without systemic overload [19,34,36], in our study no iron deposit was found in plaques of the apoE$^{-/-}$ Ct mice. However, we also detected an intense Prussian blue-positive staining in atherosclerotic plaques of the apoE$^{-/-}$ mice injected with iron, reinforcing the role of this redox-active metal ion on the atherosclerosis progression, which via pro-oxidant and pro-inflammatory effects could potentiate the atherosclerotic lesion and turn it more susceptible to rupture [1,18,36]. A pro-inflammatory profile associated with changes in the expression and/or activity of matrix metalloproteinase and cysteine proteases have been shown as important players in the vascular remodeling and atherosclerosis [37–39]. Regarding this, it was recently reported that increased dipeptidy peptidase-4, a cysteine protease, is involved in the inflammatory process

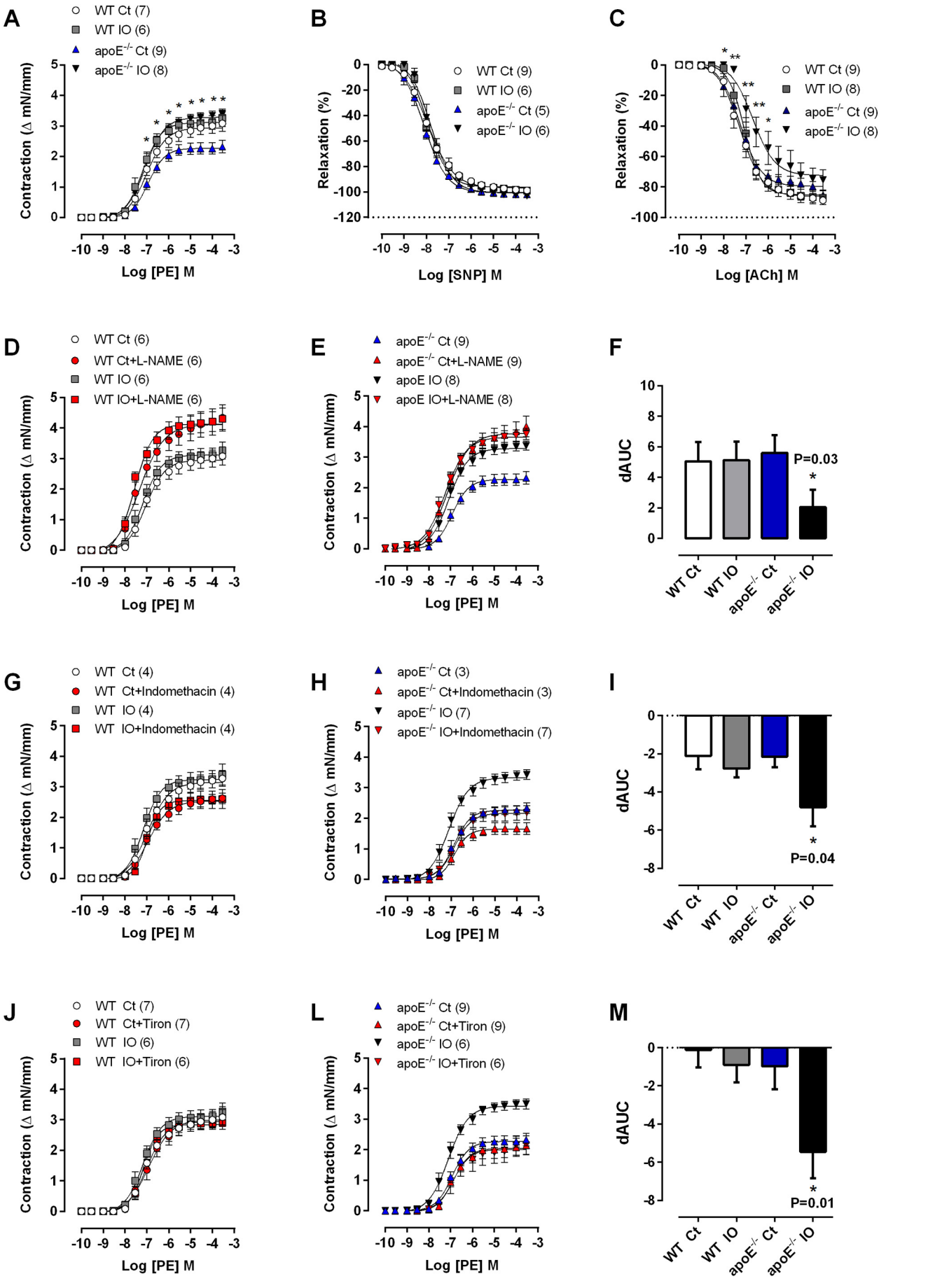

(caption on next page)

Fig. 3. Effects of chronic iron overload on vascular reactivity and endothelial modulation in the aorta. Concentration–response curves to phenylephrine (A), sodium nitroprusside (B) and acetylcholine (C) were constructed in aortic rings from the wild-type (WT) and apoE$^{-/-}$ lineages as control (Ct) and iron overload (IO) groups. Effects of incubation with 100 μM L-NAME (D-F), 10 μM indomethacin (G-I) or 1 mM tiron (J-M) on the contractile response to phenylephrine were assessed and the magnitude of the effect was measured as the difference between areas under curves with and without intervention (dAUC). PE: phenylephrine, ACh: acetylcholine, SNP: sodium nitroprusside. Data are expressed as mean ± SEM. *$P < 0.05$ and **$P < 0.01$ apoE$^{-/-}$ IO vs. apoE$^{-/-}$ Ct, by two-way ANOVA and Fisher's test for multiple comparisons. The number of animals is indicated in parentheses.

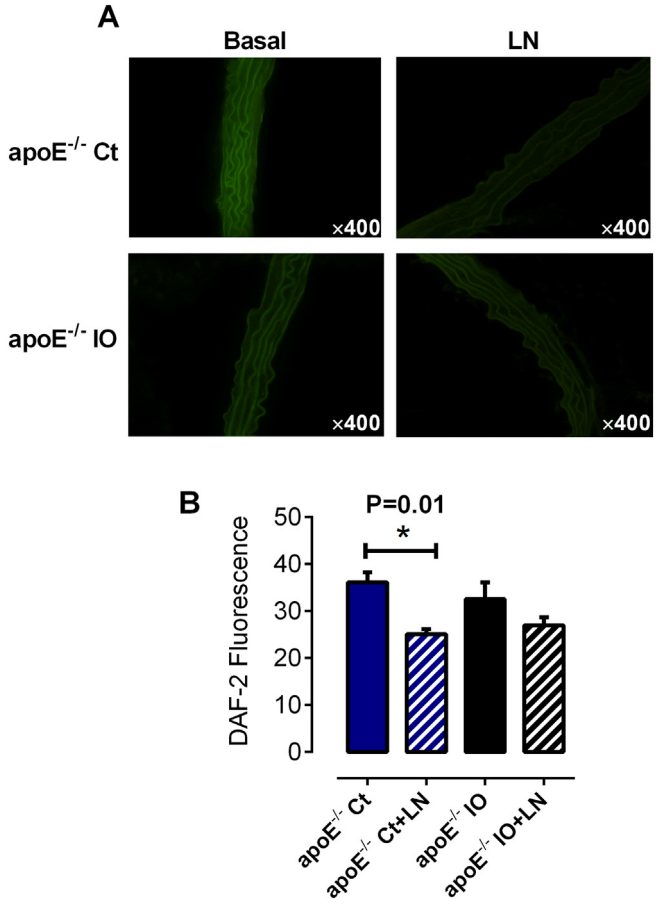

Fig. 4. *In situ* detection of NO in aortic segments of atherosclerotic mice. In A, fluorescence photomicrographies represent aortic sections in the presence of the NO-sensitive fluorescent probe 4,5-diaminufluorecein (DAF-2) from apoE$^{-/-}$ control mice (Ct) and submitted to iron overload (IO). The specificity of the method was assessed by incubating the aortas with L-NAME (LN, 100 μM). In B, bar graph demonstrating the semiquantitative analysis. Data are expressed as mean ± SEM of fluorescence density. *$P < 0.05$ indicates significant effect of LN incubation only in the apoE$^{-/-}$ Ct, by two-way ANOVA and Fisher's test for multiple comparisons. The number of animals was 4–6 per group.

and vascular dysfunction [40] and atherosclerosis of apoE$^{-/-}$ mice under chronic stress [41].

Although atherosclerosis is a multifactorial disease, current studies emphasize the central role of endothelial dysfunction associated with oxidative stress [42,43]. In fact, our data indicated that the exacerbated atherosclerosis found in the apoE$^{-/-}$ IO group was accompanied by significant endothelial dysfunction, as evidenced *in vitro* by impaired acetylcholine-induced relaxation (endothelium dependent) and increased vasocontractile response to phenylephrine. Confirming, the analysis of the endothelial surface by scanning electron microscopy demonstrated more severe damage in the apoE$^{-/-}$ IO group. Interestingly, iron overload did not change vascular reactivity of the aortic rings from WT mice. About this, the suggestion that females and C57BL-6 mice are less susceptible to iron-induced injury [44,45] could explain why despite the increased oxidative stress and vascular iron deposits, the WT IO group showed only discreet morphological changes and preserved endothelial-dependent relaxation. Regardless these changes on the endothelium-dependent vasoactivity of the apoE$^{-/-}$ IO group, the endothelium-independent relaxation to the NO donor sodium nitroprusside was similar to the other groups, suggesting that vascular smooth muscle was still preserved.

Because endothelial dysfunction is characterized by the imbalance between contractile and relaxant endothelial-derived factors, we investigated important pathways involved in the endothelial modulation of the vascular tone. Incubation with the nonspecific NOS inhibitor L-NAME increased the response to phenylephrine in all groups, but in a lesser extent in aortas of the apoE$^{-/-}$ IO mice, which suggests an impairment of the ability of NO to modulate the vascular reactivity. Corroborating the functional data, the *in situ* detection of NO releasing using a NO-sensitive probe indicated a reduced vascular NO bioavailability induced by iron overload, similar to we described previously in rats [8,9,12]. Moreover, the reversion of altered vascular function with tiron suggested that an increased ROS could be reacting with NO and reducing its action. Actually, it is well known that oxidative stress can damage the vascular endothelium, by reducing NO bioavailability and increasing platelet aggregation, leukocyte adhesion, and apoptosis, as well as the media layer, by altering smooth muscle cell proliferation and hypertrophy, stimulating inflammatory mediators and extracellular matrix disorganization, apoptosis, thereby altering the vascular tone [13,46]. Since oxidative stress is characterized by an imbalance between ROS production and antioxidant capacity, and it has been demonstrated that chronic iron injections in rodents usually decrease antioxidant defense mechanisms, such as SOD and catalase in blood and liver [47,48], we evaluated the activity of these enzymes in the aorta. Our results demonstrate that iron overload reduced SOD and catalase activities in aorta of apoE$^{-/-}$ IO mice, which may have contributed to the increase of the oxidative stress.

In human and animal models, an increase of COX-derived vasoconstrictor factors released by the dysfunctional endothelium has been associated with the development and/or maintenance of cardiovascular complications such as atherosclerosis and hypertension [49–51]. We found that acute incubation with the non-selective COX inhibitor indomethacin attenuated vascular contractions to phenylephrine in all groups, but in a greater extent in the apoE$^{-/-}$ IO group, which suggests a role for the COX-derived prostanoids. Confirming functional data, there were increased expression of COX-2 in the aorta, as well as an increased urinary level of TXA_2 in apoE$^{-/-}$ IO mice. PGIM levels also increased in the urine of the apoE$^{-/-}$ IO group, which may be a compensatory mechanism via PGI_2-mediated vasodilatation, or even a contributor to the vascular hyperreactivity since under certain conditions, high concentrations of PGI_2 may also activate TP receptor in the smooth muscle cells [52]. Notwithstanding, previous studies have demonstrated strong evidences for a role of TXA_2 in the development of atherosclerosis in apoE$^{-/-}$ mice [53,54]. Moreover, about the relationship between iron overload and COX, Mattera et al. found that rat cardiomyocytes exposed to high concentrations of iron citrate enhances COX-2 induction and its metabolites production [55] and Li et al. using chronic iron loading in thromboxane synthase knockout mice (TXAS$^{-/-}$) described that TXA_2 mediates the iron-overload cardiomyopathy [21]. Thus, we propose that an increased COX-2-derived TXA_2 in the vascular system is, at least in part, implicated in the genesis of endothelial dysfunction and the potentiation of atherosclerosis during chronic iron overload.

Among the various elements involved in the control of iron

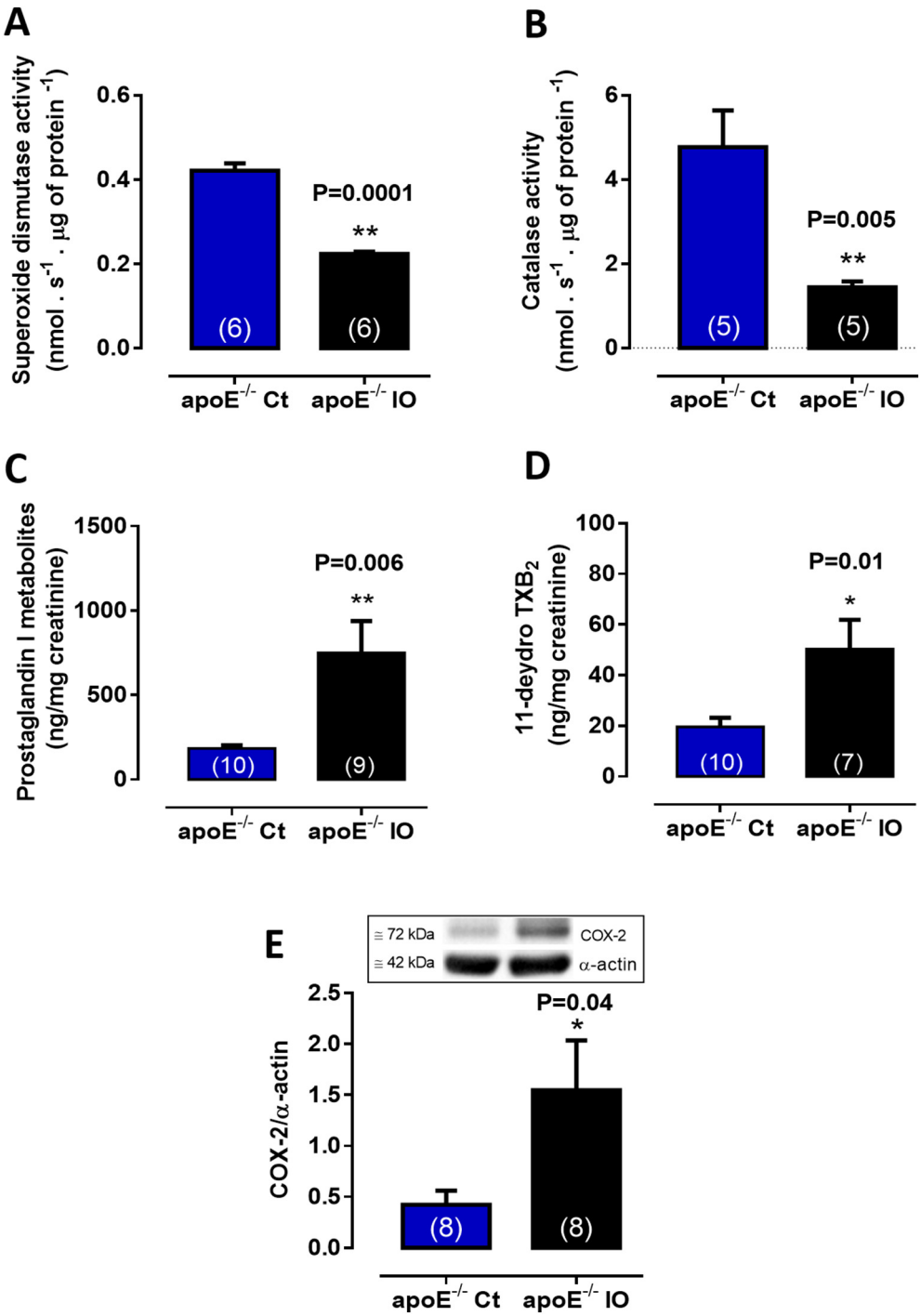

Fig. 5. Effects of iron overload on COX-2 expression, prostanoids production and antioxidant enzymes activity. Catalase (A) and superoxide dismutase (B) activities and COX-2 expression (E) were measured in the aorta. In C and D, the metabolites of prostacyclin and thromboxane A_2, respectively, were measured in urine samples from apoE$^{-/-}$ control mice (Ct) and submitted to iron overload (IO). Data are expressed as mean ± SEM. *$P < 0.05$ apoE$^{-/-}$ IO vs. apoE$^{-/-}$ Ct, by Student's *t*-test. The number of animals is indicated in parentheses.

metabolism, the interaction between hepcidin and ferroportin may have potential relevance in this oxidative stress associated with endothelial dysfunction and atherosclerosis progression. Because hepcidin inhibits the iron export through ferroportin from enterocytes and reticuloendothelial cells, including macrophages of the atherosclerotic plaques, it has been proposed that increased hepcidin might play a role in plaque instability and inflammation by increasing iron trapping and mediating lipid peroxidation and phenotypic switching of the foam cells [56,57]. As a result, we could speculate that an elevation of hepcidin in the apoE$^{-/-}$ mice in response to iron overload would stimulate iron loading into the machophages by reducing its ferroportin-mediated export, thereby intensifying oxidative stress, inflammation and structural/functional damages we found in this study.

Finally, the local irritation caused by chronic intraperitoneal injections of iron-dextran could trigger an inflammatory response that, in turn, would lead to such vascular damage and the progression of atherosclerosis. Because we did not evaluate the peritoneal exudate for inflammatory cells or cytokines, this should be a limitation of the present study. However, it is important to note that the ability to stimulate a pro-inflammatory state is inherent to the iron loading per se,

and occurs regardless of the intraperitoneal injections, such as in patients with hemochromatosis or genetic model of iron overload [35].

5. Conclusions

Our results indicate that chronic iron overload actually enhances the atherosclerotic process in apoE$^{-/-}$ mice, probably as result of exacerbated hypercholesterolemia and structural/functional endothelial damages. While iron-mediated liver injury may explain this further elevation of lipidemia, the oxidative stress and decreased NO bioavailability associated with COX-2-derived prostanoids appear to be the pathogenic substrates of endothelial dysfunction associated with iron overload in apoE$^{-/-}$ mice. Based on the current knowledge, future studies are needed to determine whether interruption in this causal connection between iron and cardiovascular disease can be beneficial, either by reducing iron levels in hypercholesterolemic subjects or by reducing atherosclerosis-related risk factors in patients with primary or secondary iron overloads.

CRediT authorship contribution statement

Vinícius Bermond Marques: Conceptualization, Investigation, Data curation, Visualization, Funding acquisition, Writing - original draft, Writing - review & editing. **Marcos André Soares Leal:**Conceptualization, Investigation, Formal analysis, Data curation. **Jandinay Gonzaga Alexandre Mageski:**Conceptualization, Investigation, Data curation. **Helbert Gabriel Fidelis:**Conceptualization, Investigation, Data curation, Writing - original draft. **Breno Valentim Nogueira:**Resources, Investigation, Data curation, Writing - review & editing. **Elisardo Corral Vasquez:**Resources, Methodology, Formal analysis, Writing - original draft. **Silvana dos Santos Meyrelles:**Conceptualization, Resources, Methodology, Formal analysis, Writing - original draft. **Maylla Ronacher Simões:**Methodology, Validation, Formal analysis, Investigation, Data curation. **Leonardo dos Santos:**Conceptualization, Formal analysis, Resources, Visualization, Supervision, Writing - review & editing, Project administration, Funding acquisition.

Declaration of Competing Interest

The authors declare that there are no conflicts of interest.

Acknowledgements

The authors would also like to thank the technical support of the Laboratory of Experimental Physiology and Biochemistry (LAFIBE – CEFD/UFES), the Laboratory of Cellular Ultrastructure Carlos Alberto Redins and the Laboratory of Molecular Histology and Immunohistochemical (Health Sciences Center UFES), by the use of the equipment for histological processing and analysis. This work was supported by grants from the Coordenação de Aperfeiçoamento de Pessoal de Nível Superior (CAPES – Finance code 001); Conselho Nacional de Desenvolvimento Científico e Tecnológico (grant number 303077/2017-4 CNPq 2018-20); and Fundação de Amparo a Pesquisa do Espírito Santo (grant numbers 80707483 and 80856756 - Edital Universal FAPES 03/2017). BVN is supported by CNPq fellowship (process number 315017/2018-0). The funders had no role in study design, data collection and analysis, decision to publish, or preparation of the manuscript.

Appendix A. Supplementary data

Supplementary data to this article can be found online at https://doi.org/10.1016/j.lfs.2019.116702.

References

[1] A. Gudjoncik, C. Guenancia, M. Zeller, Y. Cottin, C. Vergely, L. Rochette, Iron, oxidative stress, and redox signaling in the cardiovascular system, Mol. Nutr. Food Res. 58 (2014) 1721–1738, https://doi.org/10.1002/mnfr.201400036.
[2] T. Ganz, Systemic iron homeostasis, Physiol. Rev. 93 (2013) 1721–1741, https://doi.org/10.1152/physrev.00008.2013.
[3] L.L. Dunn, Y.S. Rahmanto, D.R. Richardson, Iron uptake and metabolism in the new millennium, Trends Cell Biol. 17 (2007) 93–100, https://doi.org/10.1016/j.tcb.2006.12.003.
[4] A. Siddique, K.V. Kowdley, Review article: the iron overload syndromes, Aliment. Pharmacol. Ther. 35 (2012) 876–893, https://doi.org/10.1111/j.1365-2036.2012.05051.x.
[5] S.M. Day, Chronic iron administration increases vascular oxidative stress and accelerates arterial thrombosis, Circulation 107 (2003) 2601–2606, https://doi.org/10.1161/01.CIR.0000066910.02844.D0.
[6] G.Y. Oudit, M.G. Trivieri, N. Khaper, T. Husain, G.J. Wilson, P. Liu, M.J. Sole, P.H. Backx, Taurine supplementation reduces oxidative stress and improves cardiovascular function in an iron-overload murine model, Circulation 109 (2004) 1877–1885, https://doi.org/10.1161/01.CIR.0000124229.40424.80.
[7] E.M. Rossi, V.B. Marques, D. de O. Nunes, M.T.W.D. Carneiro, P.L. Podratz, E. Merlo, L. dos Santos, J.B. Graceli, Acute iron overload leads to hypothalamic-pituitary-gonadal axis abnormalities in female rats, Toxicol. Lett. 240 (2016) 196–213, https://doi.org/10.1016/j.toxlet.2015.10.027.
[8] R.F. Ribeiro Júnior, V.B. Marques, D.O. Nunes, I. Stefanon, L. dos Santos, Chronic iron overload induces functional and structural vascular changes in small resistance arteries via NADPH oxidase-dependent O2[rad] − production, Toxicol. Lett. 279 (2017) 43–52, https://doi.org/10.1016/j.toxlet.2017.07.497.
[9] V.B. Marques, T.B. Nascimento, R.F. Ribeiro, G.B. Broseghini-Filho, E.M. Rossi, J.B. Graceli, L. dos Santos, Chronic iron overload in rats increases vascular reactivity by increasing oxidative stress and reducing nitric oxide bioavailability, Life Sci. 143 (2015) 89–97, https://doi.org/10.1016/j.lfs.2015.10.034.
[10] H. Gaenzer, P. Marschang, W. Sturm, G. Neumayr, W. Vogel, J. Patsch, G. Weiss, Association between increased iron stores and impaired endothelial function in patients with hereditary hemochromatosis, J. Am. Coll. Cardiol. 40 (2002) 2189–2194, https://doi.org/10.1016/S0735-1097(02)02611-6.
[11] J. Lekakis, C. Papamicheal, K. Stamatelopoulos, A. Cimponeriu, A. Voutsas, K. Vemmos, M. Mavrikakis, S. Stamatelopoulos, Hemochromatosis associated with endothelial dysfunction: evidence for the role of iron stores in early atherogenesis, Vasc. Med. 4 (1999) 147–148, https://doi.org/10.1177/1358836X9900400305.
[12] S.R. Bertoli, V.B. Marques, E.M. Rossi, M. Krause, M.T.W.D. Carneiro, M.R. Simões, L. dos Santos, Chronic iron overload induces vascular dysfunction in resistance pulmonary arteries associated with right ventricular remodeling in rats, Toxicol. Lett. 295 (2018) 296–306, https://doi.org/10.1016/j.toxlet.2018.07.010.
[13] A.C. Montezano, R.M. Touyz, Reactive oxygen species and endothelial function - role of nitric oxide synthase uncoupling and nox family nicotinamide adenine dinucleotide phosphate oxidases, Basic Clin. Pharmacol. Toxicol. 110 (2012) 87–94, https://doi.org/10.1111/j.1742-7843.2011.00785.x.
[14] X.M. Xie, X. Cao, M.F. Chen, Y.C. Zhou, X. Bin Chen, H.Y. Jiang, Effect of chronic iron overload on atherosclerosis lesion in apolipoprotein E knockout mice, J. Cent. South Univ. (Medical Sci.) (2008). doi:1672-7347(2008)01-0057-06 (pii).
[15] J.A. Araujo, E.L. Romano, B.E. Brito, V. Parthé, M. Romano, M. Bracho, R.F. Montaño, J. Cardier, Iron overload augments the development of atherosclerotic lesions in rabbits, Arterioscler. Thromb. Vasc. Biol. 15 (1995) 1172–1180, https://doi.org/10.1161/01.ATV.15.8.1172.
[16] L. Kautz, V. Gabayan, X. Wang, J. Wu, J. Onwuzurike, G. Jung, B. Qiao, A.J. Lusis, T. Ganz, E. Nemeth, Testing the iron hypothesis in a mouse model of atherosclerosis, Cell Rep. 5 (2013) 1436–1442, https://doi.org/10.1016/j.celrep.2013.11.009.
[17] E.A. Kirk, J.W. Heinecke, R.C. LeBoeuf, Iron overload diminishes atherosclerosis in apoE-deficient mice, J. Clin. Invest. 107 (2001) 1545–1553, https://doi.org/10.1172/JCI7664.
[18] F. Vinchi, M.U. Muckenthaler, M.C. Da Silva, G. Balla, J. Balla, V. Jeney, Atherogenesis and iron: from epidemiology to cellular level, Front. Pharmacol. (2014) 1–20, https://doi.org/10.3389/fphar.2014.00094 5 MAY.
[19] J. Swain, J.M.C. Gutteridge, Prooxidant iron and copper, with ferroxidase and xanthine oxidase activities in human atherosclerotic material, FEBS Lett. 368 (1995) 513–515, https://doi.org/10.1016/0014-5793(95)00726-P.
[20] S.S. Meyrelles, V.A. Peotta, T.M.C. Pereira, E.C. Vasquez, Endothelial dysfunction in the apolipoprotein E-deficient mouse: insights into the influence of diet, gender and aging, Lipids Health Dis. 10 (2011) 211, https://doi.org/10.1186/1476-511X-10-211.
[21] H. Lin, H.-F. Li, W.-S. Lian, H.-H. Chen, Y.-F. Lan, P.-F. Lai, C.-F. Cheng, Thromboxane A2 mediates iron-overload cardiomyopathy in mice through Calcineurin-nuclear factor of activated T cells signaling pathway, Circ. J. 77 (2013) 2586–2595, https://doi.org/10.1253/circj.CJ-12-1516.
[22] X. Gao, M. Qian, J.L. Campian, J. Marshall, Z. Zhou, A.M. Roberts, Y.J. Kang, S.D. Prabhu, X.F. Sun, J.W. Eaton, Mitochondrial dysfunction may explain the cardiomyopathy of chronic iron overload, Free Radic. Biol. Med. 49 (2010) 401–407, https://doi.org/10.1016/j.freeradbiomed.2010.04.033.
[23] R.F. Ribeiro, F.F. Potratz, B.M.M. Pavan, L. Forechi, F.L.M. Lima, J. Fiorim, A.A. Fernandes, D.V. Vassallo, I. Stefanon, Carvedilol prevents ovariectomy-induced myocardial contractile dysfunction in female rat, PLoS One 8 (2013), https://doi.org/10.1371/journal.pone.0053226.
[24] P.V.C. Zovico, V.M. Curty, M.A.S. Leal, E.F. Meira, D.V. Dias, L.C. de M. Rodrigues,

S. dos S. Meyrelles, E.M. De Oliveira, P.F. Vassallo, V.G. Barauna, Effects of controlled doses of Oxyelite pro on physical performance in rats, Nutr. Metab. 13 (2016) 1–10, https://doi.org/10.1186/s12986-016-0152-4.
[25] A.G.F. Friques, C.M. Arpini, I.C. Kalil, A.L. Gava, M.A. Leal, M.L. Porto, B.V. Nogueira, A.T. Dias, T.U. Andrade, T.M.C. Pereira, S.S. Meyrelles, B.P. Campagnaro, E.C. Vasquez, Chronic administration of the probiotic kefir improves the endothelial function in spontaneously hypertensive rats, J. Transl. Med. 13 (2015) 1–16, https://doi.org/10.1186/s12967-015-0759-7.
[26] M.J. Mulvany, W. Halpern, Contractile properties of small arterial resistance vessels in spontaneously hypertensive and normotensive rats, Circ. Res. 41 (1977) 19–26, https://doi.org/10.1161/01.RES.41.1.19.
[27] S.N. Moon, J.W. Han, H.S. Hwang, M.J. Kim, S.J. Lee, J.Y. Lee, C.K. Oh, D.C. Jeong, Establishment of secondary iron overloaded mouse model: Evaluation of cardiac function and analysis according to iron concentration, Pediatr. Cardiol. 32 (2011) 947–952, https://doi.org/10.1007/s00246-011-0019-4.
[28] L.X. Lou, B. Geng, Y. Chen, F. Yu, J. Zhao, C.S. Tang, Endoplasmic reticulum stress involved in heart and liver injury in iron-loaded rats, Clin. Exp. Pharmacol. Physiol. 36 (2009) 612–618, https://doi.org/10.1111/j.1440-1681.2008.05114.x.
[29] B.R. Bacon, R.S. Britton, The pathology of hepatic iron overload: a free radical-mediated process? Hepatology (1990), https://doi.org/10.1002/hep.1840110122.
[30] A.S. Plump, J.D. Smith, T. Hayek, K. Aalto-Setälä, A. Walsh, J.G. Verstuyft, E.M. Rubin, J.L. Breslow, Severe hypercholesterolemia and atherosclerosis in apolipoprotein E-deficient mice created by homologous recombination in ES cells, Cell 71 (1992) 343–353, https://doi.org/10.1016/0092-8674(92)90362-G.
[31] Y. Nakashima, A.S. Plump, E.W. Raines, J.L. Breslow, R. Ross, ApoE-deficient mice develop lesions of all phases of atherosclerosis throughout the arterial tree, Arterioscler. Thromb. Vasc. Biol. 14 (1994) 133–140, https://doi.org/10.1161/01.ATV.14.1.133.
[32] R. Minqin, R. Rajendran, N. Pan, B.K.H. Tan, W.Y. Ong, F. Watt, B. Halliwell, The iron chelator desferrioxamine inhibits atherosclerotic lesion development and decreases lesion iron concentrations in the cholesterol-fed rabbit, Free Radic. Biol. Med. 38 (2005) 1206–1211, https://doi.org/10.1016/j.freeradbiomed.2005.01.008.
[33] T.S. Lee, M.S. Shiao, C.C. Pan, L.Y. Chau, Iron-deficient diet reduces atherosclerotic lesions in ApoE-deficient mice, Circulation 99 (1999) 1222–1229, https://doi.org/10.1161/01.CIR.99.9.1222.
[34] W.J. Zhang, H. Wei, B. Frei, The iron chelator, desferrioxamine, reduces inflammation and atherosclerotic lesion development in experimental mice, Exp. Biol. Med. 235 (2010) 633–641, https://doi.org/10.1258/ebm.2009.009229.
[35] F. Vinchi, G. Porto, A. Simmelbauer, S. Altamura, S.T. Passos, M. Garbowski, A.M.N. Silva, S. Spaich, S.E. Seide, R. Sparla, M.W. Hentze, M.U. Muckenthaler, Atherosclerosis is aggravated by iron overload and ameliorated by dietary and pharmacological iron restriction, Eur. Heart J. (2019) 1–16, https://doi.org/10.1093/eurheartj/ehz112.
[36] J.B. Michel, R. Virmani, E. Arbustini, G. Pasterkamp, Intraplaque haemorrhages as the trigger of plaque vulnerability, Eur. Heart J. 32 (2011) 1977–1985, https://doi.org/10.1093/eurheartj/ehr054.
[37] G. Yang, Y. Lei, A. Inoue, L. Piao, L. Hu, H. Jiang, T. Sasaki, H. Wu, W. Xu, C. Yu, G. Zhao, S. Ogasawara, K. Okumura, M. Kuzuya, X.W. Cheng, Exenatide mitigated diet-induced vascular aging and atherosclerotic plaque growth in ApoE-deficient mice under chronic stress, Atherosclerosis 264 (2017) 1–10, https://doi.org/10.1016/j.atherosclerosis.2017.07.014.
[38] X.W. Cheng, G.P. Shi, M. Kuzuya, T. Sasaki, K. Okumura, T. Murohara, Role for cysteine protease cathepsins in heart disease: Focus on biology and mechanisms with clinical implication, Circulation 125 (2012) 1551–1562, https://doi.org/10.1161/CIRCULATIONAHA.111.066712.
[39] X.W. Cheng, Z. Huang, M. Kuzuya, K. Okumura, T. Murohara, Cysteine protease cathepsins in atherosclerosis-based vascular disease and its complications, Hypertension 58 (2011) 978–986, https://doi.org/10.1161/HYPERTENSIONAHA.111.180935.
[40] B.C. de Oliveira, V.B. Marques, B.F. Brun, H.M. de Oliveira e Silva, S. Freitas Soares Melo, E.M. de Oliveira, L. dos Santos, V.G. Barauna, Dipeptidyl peptidase-4 inhibition prevents vascular dysfunction induced by β-adrenergic hyperactivity, Biomed. Pharmacother. 113 (2019) 108733, https://doi.org/10.1016/j.biopha.2019.108733.
[41] Y. Lei, G. Yang, L. Hu, L. Piao, A. Inoue, H. Jiang, T. Sasaki, G. Zhao, M. Yisireyili, C. Yu, W. Xu, K. Takeshita, K. Okumura, M. Kuzuya, X.W. Cheng, Increased dipeptidyl peptidase-4 accelerates diet-related vascular aging and atherosclerosis in ApoE-deficient mice under chronic stress, Int. J. Cardiol. 243 (2017) 413–420, https://doi.org/10.1016/j.ijcard.2017.05.062.
[42] K. Bishu, R. Agarwal, Acute injury with intravenous iron and concerns regarding long-term safety, Clin. J. Am. Soc. Nephrol. 1 (Suppl. 1) (2006) 19–23, https://doi.org/10.2215/CJN.01420406.
[43] E. Schulz, T. Jansen, P. Wenzel, A. Daiber, T. Münzel, Nitric oxide, tetrahydrobiopterin, oxidative stress, and endothelial dysfunction in hypertension, Antioxid. Redox Signal. 10 (2008) 1115–1126, https://doi.org/10.1089/ars.2007.1989.
[44] M. Musumeci, S. Maccari, P. Sestili, A. Massimi, E. Corritore, G. Marano, L. Catalano, The C57BL/6 genetic background confers cardioprotection in iron-overloaded mice, Blood Transfus. 11 (2013) 88–93, https://doi.org/10.2450/2012.0176-11.
[45] S.K. Das, V.B. Patel, R. Basu, W. Wang, J. DesAulniers, Z. Kassiri, G.Y. Oudit, Females are protected from iron-overload cardiomyopathy independent of iron metabolism: key role of oxidative stress, J. Am. Heart Assoc. 6 (2017) 11–13, https://doi.org/10.1161/JAHA.116.003456.
[46] K. Irani, Oxidant signaling in vascular cell growth, death, and survival, Circ. Res. 87 (2000) 179–183, https://doi.org/10.1007/s00373-007-0721-4.
[47] F.A. Badria, A.S. Ibrahim, A.F. Badria, A.A. Elmarakby, Curcumin attenuates iron accumulation and oxidative stress in the liver and spleen of chronic iron-overloaded rats, PLoS One 10 (2015), https://doi.org/10.1371/journal.pone.0134156.
[48] Z. Zhang, D. Liu, B. Yi, Z. Liao, L. Tang, D. Yin, M. He, Taurine supplementation reduces oxidative stress and protects the liver in an iron-overload murine model, Mol. Med. Rep. 10 (2014) 2255–2262, https://doi.org/10.3892/mmr.2014.2544.
[49] M. Félétou, Y. Huang, P.M. Vanhoutte, Endothelium-mediated control of vascular tone: COX-1 and COX-2 products, Br. J. Pharmacol. 164 (2011) 894–912, https://doi.org/10.1111/j.1476-5381.2011.01276.x.
[50] S. Li, B. Liu, W. Luo, Y. Zhang, H. Li, D. Huang, Y. Zhou, Role of cyclooxygenase-1 and -2 in endothelium-dependent contraction of atherosclerotic mouse abdominal aortas, Clin. Exp. Pharmacol. Physiol. 43 (2016) 67–74, https://doi.org/10.1111/1440-1681.12501.
[51] L. Dos Santos, F.E. Xavier, D.V. Vassallo, L.V. Rossoni, Cyclooxygenase pathway is involved in the vascular reactivity and inhibition of the Na+, K+-ATPase activity in the tail artery from L-NAME-treated rats, Life Sci. 74 (2003) 613–627, https://doi.org/10.1016/j.lfs.2003.07.002.
[52] M. Félétou, T.J. Verbeuren, P.M. Vanhoutte, Endothelium-dependent contractions in SHR: a tale of prostanoid TP and IP receptors, Br. J. Pharmacol. 156 (2009) 563–574, https://doi.org/10.1111/j.1476-5381.2008.00060.x.
[53] A.J. Cayatte, Y. Du, J. Oliver-Krasinski, G. Lavielle, T.J. Verbeuren, R.A. Cohen, The thromboxane receptor antagonist S18886 but not aspirin inhibits atherogenesis in apoE-deficient mice: evidence that eicosanoids other than thromboxane contribute to atherosclerosis, Arterioscler. Thromb. Vasc. Biol. 20 (2000) 1724–1728, https://doi.org/10.1161/01.ATV.20.7.1724.
[54] T. Kobayashi, T. Kita, S. Narumiya, T. Kobayashi, Y. Tahara, M. Matsumoto, M. Iguchi, H. Sano, Roles of Thromboxane a 2 and Prostacyclin in the Development of Atherosclerosis in apoE- Deficient Mice find the Latest Version : Roles of Thromboxane a 2 and Prostacyclin in the Development of Atherosclerosis in apoE-Deficient Mice, 114 (2004), pp. 784–794, https://doi.org/10.1172/JCI200421446.784.
[55] R. Mattera, G.P. Stone, N. Bahhur, Y.A. Kuryshev, Increased release of arachidonic acid and eicosanoids in iron-overloaded cardiomyocytes, Circulation 103 (2001) 2395–2401, https://doi.org/10.1161/01.CIR.103.19.2395.
[56] J.J. Li, X. Meng, H.P. Si, C. Zhang, H.X. Lv, Y.X. Zhao, J.M. Yang, M. Dong, K. Zhang, S.X. Liu, X.Q. Zhao, F. Gao, X.L. Liu, T.X. Cui, Y. Zhang, Hepcidin destabilizes atherosclerotic plaque via overactivating macrophages after erythrophagocytosis, Arterioscler. Thromb. Vasc. Biol. 32 (2012) 1158–1166, https://doi.org/10.1161/ATVBAHA.112.246108.
[57] O. Saeed, F. Otsuka, R. Polavarapu, V. Karmali, D. Weiss, T. Davis, B. Rostad, K. Pachura, L. Adams, J. Elliott, W.R. Taylor, J. Narula, F. Kolodgie, R. Virmani, C.C. Hong, A.V. Finn, Pharmacological suppression of hepcidin increases macrophage cholesterol efflux and reduces foam cell formation and atherosclerosis, Arterioscler. Thromb. Vasc. Biol. 32 (2012) 299–307, https://doi.org/10.1161/ATVBAHA.111.240101.